Nanoparticle effects on the water-oil interfacial tension

Heng Fan and Alberto Striolo

Phys. Rev. E **86**, 051610 — Published 29 November 2012

DOI: 10.1103/PhysRevE.86.051610

Nanoparticles Effects on the Water-Oil Interfacial Tension

Heng Fan and Alberto Striolo*

The University of Oklahoma

School of Chemical, Biological, and Materials Engineering

Norman, Oklahoma 73019

Although it is well known that solid particles adsorb at interfaces, no consensus has been reached on whether or not the adsorbed nanoparticles affect interfacial tension. In this work the Wilhelmy plate method is implemented in mesoscale dissipative particle dynamics (DPD) simulations to study the influence of nanoparticles on the water-oil interfacial tension. The results are compared with predictions that neglect nanoparticle-nanoparticle interactions at the interface. We find that the two estimates can differ significantly. In the regime where nanoparticle-nanoparticle repulsion is large, the Wilhelmy plate method suggests interfacial tension reduction, which appears to be a strong function of nanoparticle surface coverage. Some experimental data from the literature, in apparent disagreement, are re-interpreted based on this insight.

* Author to whom correspondence should be addressed: astriolo@ou.edu

1. Introduction

It is well known that nanoparticles with suitable size and surface chemistry strongly adsorb at liquid-liquid and/or liquid-air interfaces. It is accepted that this phenomenon occurs because the adsorption lowers the total system energy. However, there is a long ongoing debate on whether or not nanoparticles (NPs) adsorbed at an interface can reduce the interfacial tension.[1-11] Briefly, Johnson and Dong studied the interfacial tension of charge-stabilized TiO_2 dispersions at high pH. They found that as the particle concentration in the system increases the interfacial tension first decreases, but then increases to values even larger than those observed in the absence of nanoparticles.[1] Glaser et al. found that Au-Fe_3O_4 Janus nanoparticles can more significantly reduce the interfacial tension than homogeneous ones at similar concentrations.[10] Okubo investigated the water-air interfacial tension in the presence of polystyrene and silica particles. The interfacial tension was found to reduce significantly only when the polystyrene particles self-assembled yielding crystalline structures at the interfaces. In the other cases (silica particles at the interface, independently on the structure formed, or polystyrene particles not yielding crystalline structures) the interfacial tension was found to remain practically equal to that of the water-air interface.[3] Vignati and Piazza measured the interfacial tension of an oil droplet in water in the presence of silica nanoparticles treated with hexamethyldisilazane. The interfacial tension was found not to change as either the nanoparticle concentration or the hydrophobicity of their surface were varied.[4] Saleh et al. reported that highly charged poly(styrenesulfonate)-grafted silica particles can significantly reduce water-oil interfacial tension while the bare silica particles do not affect the interfacial tension.[11] Blute et al. measured interfacial tensions in the presence of various types of commercial silica nanoparticles systematically changing system pH and nanoparticles concentration. The largest interfacial tension reduction reported was of only 6 mN/m, observed at low pH and high nanoparticle concentration.[5]

This short summary shows that particles are sometimes found to decrease the interfacial tension, but in some other cases they are found to not alter significantly this thermodynamic quantity. When significant interfacial tension reduction is observed, the effect is generally explained by a large particle energy of adsorption at the interface. When no change in interfacial tension is observed, the results are explained as if the particles are not 'surface active', although the particles do adsorb at the interface.

Numerous simulation studies have been reported for nanoparticles at interfaces. Yang et al.,[12] using dissipative particle dynamic (DPD) simulations, found that nano-rods can reduce the interfacial tension and increase the thickness of the interface in incompatible polymer blends. The interfacial tension in the presence of hydroxylated SiO_2 nanoparticles at various temperatures, salt types, and salt concentrations was also investigated, both experimentally and computationally.[13] It was found that the different propensity of the ions to distribute on the NPs surface affects the interfacial tension. Ranatunga et al. simulated NPs and non-ionic surfactants at the oil-water interface using molecular dynamics.[14] At low concentrations surfactants and NPs show cooperative behavior in reducing the interfacial tension. However, as the concentration increases, adsorption onto the NP surface decreases the surfactant efficiency in lowering the interfacial tension, while concurrently preventing NP aggregation. Luo and Dai,[15] conducting simulations, found that surfactants and NPs compete for adsorption at liquid-liquid interfaces, and that as the surfactant concentration increased the NPs desorb from the interface. The thickness of the interface and the interfacial tension were found to depend significantly on the surfactant concentration, but not so on the NP adsorption.

The goal of the present study is to quantify whether a given particle can or cannot reduce the interfacial tension of the water-oil interface, using dissipative particle dynamics (DPD). The interfacial tension is the force parallel to the interface but perpendicular to a line of unit length.[16] Many experimental techniques are available to measure interfacial tension (e.g., Du Nouy ring, Wilhelmy plate, pendant drop experiments, and others).[17] To calculate the interfacial tension at the water-decane interface we implement here an algorithm that reproduces the experimental Wilhelmy plate method. The algorithm is implemented using DPD simulations and the results are referred to as 'mechanical interfacial tension' within this manuscript. The reliability of the algorithm is demonstrated by reproducing interfacial tension results obtained from the widely employed pressure-tensor method.[18] Computationally, the interfacial tension can also be calculated as the work necessary to generate a unit interfacial area. Assuming that NP-NP interactions can be neglected, the interfacial tension (γ_C) can be estimated as:[19]

$$\gamma_C = \gamma_0 - N_p E_d / A \qquad (1)$$

In Eq. (1) γ_0 is the interfacial tension of the bare interface, E_d is the desorption energy required to remove one nanoparticle from the interface, N_p is the number of nanoparticles in a given interfacial area A. In the remainder of this manuscript we refer to the interfacial tension calculated by Eq. (1) as the 'computational interfacial tension', hence the symbol γ_C.

Mechanical interfacial tension results obtained are compared to computational predictions based on Eq. (1), which essentially overlooks NP-NP interactions. Such interactions are found to contribute significantly to the mechanical interfacial tension, which we believe more reliably compares to experimental observations than the computational interfacial tension. Based on these molecular-level insights, we re-evaluate some of the experimental data available in the literature emphasizing the role of particle-particle interactions.

2 Simulation Methods and Algorithms

2.1 Dissipative Particle Dynamics (DPD) Simulations

Detailed descriptions of the DPD formalism are available in the literature.[20-23] The system simulated here is composed of water, oil (decane), and nanoparticles. We arbitrarily chose the 'degree of coarse graining' $N_m = 5$, with the understanding that one DPD water bead represents 5 water molecules. Within this assumption, the volume of each bead is ~ 150 $\mathring{A}^3$.

The system density is defined as the number of beads in a cube of radius R_c. We chose $\rho = 3\ beads / R_c^3$, and the interaction radius becomes $R_c = \sqrt[3]{3 \cdot 150} = 0.766\ nm$.

The volume of one decane molecule is ~0.323 nm^3. Because all DPD beads in one system are expected to have the same volume, one decane molecule has to be represented by 2 beads in our representation. To maintain the linear morphology of decane, the two beads are connected by one harmonic spring of length 0.72 R_c and spring constant $350\ k_B T / R_c$.[21]

The DPD time scale can be gauged by matching the self-diffusion constant of water. As demonstrated by Groot and Rabone,[21] the time constant of the simulation can be calculated as $\tau = \frac{N_m D_{sim} R_c^2}{D_{water}}$ where τ is the DPD time constant, D_{sim} is the simulated water self-diffusion

coefficient, and D_{water} is the experimental water self-diffusion coefficient. When $a_{w-w} = 131.5\ k_B T / R_c$ (see details below), we obtained $D_{sim} = 0.0063\ R_c^2 / \tau$. For $D_{water} = 2.43 \times 10^{-5}\ cm^2 / s$,[24] we finally obtain $\tau = 7.6\ ps$.

Following a prior work by Calvaresi et al.[25] for dispersions containing carbon nanotubes, the nanoparticles (NPs) are modeled as hollow spheres with radius of 2 R_c. One bead is maintained at the NP center and 192 beads on the NP surface. All the beads were grouped into a rigid body as they translate and rotate as a single entity. The surface beads are distributed uniformly on the surface, minimizing the maximum distance between surface beads.[26] The number of beads on the NP surface is sufficient to prevent solvent beads (water or decane) from penetrating the NP, which would be unphysical. The NP surface beads are either polar (p) or non-polar (ap). NPs of different surface chemistry are prepared by adjusting the ratio between p and ap beads on one NP surface, and by controlling their distribution (homogeneous and Janus NPs are prepared).

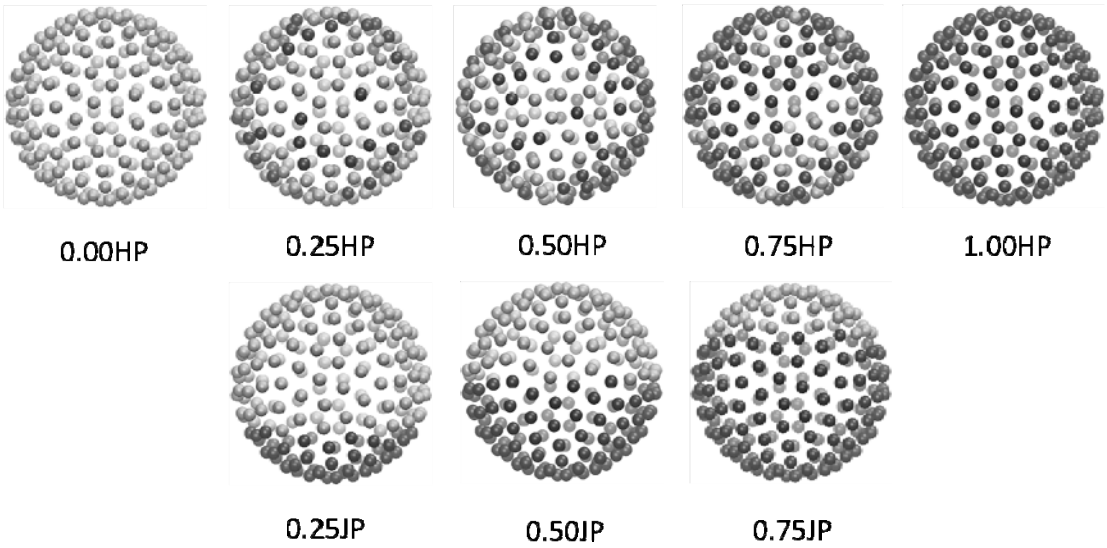

Figure 1. Schematic of the nanoparticles simulated in this work. On the top we represent the NPs with a homogeneous distribution of polar, p, and nonpolar, ap, beads on their surface. From left to right these are 0.00HP, 0.25HP, 0.50HP, 0.75HP, and 1.00 HP. On the bottom we represent Janus NPs. From left to right these are 0.25JP, 0.50JP, and 0.75JP. Lighter and darker spheres represent polar and nonpolar beads, respectively.

As shown in Fig. 1, eight NP types are simulated, all of diameter 4 R_c: (1) NPs with only p beads (0.00HP); (2) NPs with only ap beads (1.00HP); (3) homogeneous NPs composed of 96 p and 96

ap beads, randomly distributed on the surface (0.50HP); (4) homogeneous NPs with 144 p and 48 ap beads (0.25HP); (5) homogeneous NPs with 48 p and 144 ap beads (0.75HP); (6) Janus NPs with 96 p and 96 ap beads (0.50JP); (7) Janus NPs with 144 p and 48 ap beads (0.25JP); (8) Janus NPs with 48 p and 144 ap beads (0.75JP). Together with schematic representations of the various NPs, in Fig. 1 we illustrate the correspondent nomenclature. HP and JP are for homogeneous and Janus NPs, respectively. The numbers preceding HP or JP indicate the fraction of the NP beads that are nonpolar (e.g., 0.00HPs are composed solely of polar beads).

Four bead types are present in our system: water (w), oil (o), NP polar (p), NP nonpolar beads (ap). Additional bead types are introduced in the micro Wilhelmy plate (MWP) algorithm, discussed below, to describe detection plate and surfactant molecules. The bead type used in the detection plate is identified as 'detection' bead, dp. Surfactant beads are identified as head and tail beads (h and t, respectively).

Interaction parameters are needed, both intra-species (a_{i-i}) and inter-species (a_{i-j}). Groot and Warren[22] obtained a_{i-i} for water beads that reproduce the compressibility of water at ambient conditions. For $N_m = 5$ we obtain $a_{w-w} = 131.5\ k_B T / R_c$. Because water and oil beads have the same volume, and because both R_c and the pressure are constant,[23] it follows that $a_{w-w} = a_{o-o} = 131.5\ k_B T / R_c$. To simplify the parameterization, we also impose $a_{p-p} = a_{ap-ap} = 131.5\ k_B T / R_c$.

As demonstrated by Groot and Warren,[22] inter-species interaction parameter a_{i-j} can be related to Flory-Huggins parameters as $\chi_{ij} = 0.286(a_{i-j} - a_{i-i})\ (\rho = 3)$.

The oil - water Flory-Huggins parameter χ_{ow} can be obtained by $\chi_{ow} = \frac{V_{bead}}{kT}\left(\delta_o - \delta_w\right)^2$ where V_{bead} is the volume of one bead, 150 $\mathring{A}^3$ in our system; and δ_o and δ_w are the experimental solubility parameters for n-decane and water, respectively. [23] With $\delta_o = 13.5(J/cm^3)^{\frac{1}{2}}$ and $\delta_w = 47.9(J/cm^3)^{\frac{1}{2}}$,[27] we obtain $\chi_{ow} = 43.16$, which, using Eq. (2), yields $a_{o-w} = 194.7\ k_B T / R_c$.

We consider the parameter a_{o-w} just derived as a first approximation. The parameter used in our simulations is further tuned to match the experimental interfacial tension between water and n-decane, $\gamma = 51.7 mN/m$,[28] obtaining $a_{o-w} = 198.5\ k_B T / R_c$.

To parameterize a_{o-p}, a_{o-ap}, a_{w-p} and a_{w-ap} we impose that the DPD three-phase contact angles for the various NPs correspond to values obtained in atomistic molecular dynamics simulations for similar systems, with only one NP at the interface.[29] In this procedure the interaction parameter a_{p-ap} was set arbitrarily to 190 $k_B T / R_c$, similar to the oil-water interaction parameter, and the other parameters were determined iteratively. Their final values are reported in Table 1. After appropriate parameterization it was found that the 0.00HP NPs remain in the aqueous phase (as the analogous atomistic NPs did in our previous simulation,[29] which agrees with experiments), while the 1.00HP, 0.50HP, and 0.50JP NPs yield three-phase contact angles of 94.9°, 59.8°, and 84.5° respectively, in agreement with atomistic simulations.[29]

The noise parameter was set to $\lambda = 4.5$, as recommended by Groot and Warren for systems with density larger than 2 $beads / R_c^3$.[22] A time step of $\Delta t = 0.04$ was used to integrate the equations of motion. All DPD simulations were performed using the LAMMPS package.[30] Simulation box size and length of the simulations differ depending on the algorithm used for our calculations. Details are provided below as appropriate.

Table 1. Interaction parameters a_{ij} for DPD simulations, expressed in $k_B T / R_c$.

	w	**o**	**ap**	**p**	**h**	**t**	**dp**
w	131.5	198.5	178.5	110	131.5	198.5	131.5
o		131.5	161.5	218.5	198.5	131.5	131.5
ap			131.5	190	131.5	131.5	200
p				131.5	131.5	131.5	200
h					131.5	198.5	200
t						131.5	200
dp							131.5

2.2 NPs Desorption Energy

To apply Eq. (1) we require the NPs desorption energies. As discussed in our prior work,[29] we found that the following approximations are satisfactory for silica-based nanoparticles at water-decane interfaces, provided only one nanoparticle is at the interface. For homogeneous NPs:

$$E = \pi R^2 \gamma_{ow} \left(1 \pm \cos\theta_c\right)^2 \tag{2}$$

where θ_c is the three-phase contact angle and R is the NP radius. The sign within parenthesis is negative for NP removal into the water phase, and positive for removal into the oil phase.

For Janus nanoparticles, as shown by others, [31, 32] the desorption energy can be expressed in terms of three angles: θ_p, θ_a and α. θ_p and θ_a are the three-phase contact angle of NPs made solely by polar beads (0.00HP) and NPs made solely by nonpolar beads (1.00HP), respectively. α is the geometry angle of the Janus NP.[29, 31] For NPs with $\theta_p < \alpha < \theta_a$, it is assumed that $\theta_c = \alpha$, and the desorption energies can be calculated as: [31, 32]

$$E_{Oil} = 2\pi R^2 \gamma_{ow} \left[\frac{1}{2}\sin^2\alpha + \cos\theta_p (1+\cos\alpha)\right] \tag{3}$$

$$E_{Water} = 2\pi R^2 \gamma_{ow} \left[\frac{1}{2}\sin^2\alpha - \cos\theta_a (1-\cos\alpha)\right] \tag{4}$$

When $\theta_p < \theta_a < \alpha$, $\theta_c = \theta_a$, and the NPs desorption energies become:

$$E_{Oil} = 2\pi R^2 \gamma_{ow} \left[\frac{1}{2}\sin^2\theta_a + \left(1+\cos\alpha\right)\cos\theta_p + \left(\cos\theta_a - \cos\alpha\right)\cos\theta_a\right] \tag{5}$$

$$E_{Water} = \pi R^2 \gamma_{ow} \left(1-\cos\theta_a\right)^2 \tag{6}$$

Several NPs are considered in this work, as shown in Fig. 1. The three phase contact angle (θ_c) and the geometry angle (α) for all NPs are listed in Table 2. These values are obtained as averaged over all NPs surface densities considered. In general, little variation is observed in the contact angle as a function of surface coverage. In Table 2 we also report the desorption energies, expressed in $k_B T$, for desorbing the various NPs into the oil or water phases, as estimated by Eqs. (2)-(6).

Since NPs are expected to desorb from one interface into the phase (aqueous or organic) for which the correspondent desorption energy is lower, for each NP in Eq. (1) we use the smaller desorption energy. Explicitly, E_{Water} is used for all NPs except for 1.00HP NPs, for which E_{Oil} is used instead. This choice does not affect the conclusions of the present manuscript. For example, if the larger desorption energy was used instead of the smaller, the calculated interfacial tension using Eq. (1) would deviate even further compared to predictions obtained implementing the Micro Wilhelmy Plate algorithm.

Table 2. Contact angle (θ_c) and geometry angle (α),[a] and desorption energies into the oil, E_{Oil}, or the water phases, E_{Water}, for the various NPs considered in this study at the water-decane interface.[b]

	0.00HP	**0.25HP**	**0.50HP**	**0.75HP**	**1.00HP**	**0.25JP**	**0.50JP**	**0.75JP**
θ_c	0°	50.7° ±0.9°	65.4° ±0.8°	79.1° ±0.5°	94.9° ±0.6°	59.8° ±2.8°	84.5° ±0.8°	94.0° ±0.7°
α	N/A	N/A	N/A	N/A	N/A	60°	90°	120°
$E_{Oil}(\mathrm{k}_B\mathrm{T})$	N/A	245.9	184.9	130.2	76.9	345.4	276.3	177.0
$E_{Water}(\mathrm{k}_B\mathrm{T})$	N/A	12.3	31.3	60.6	108.6	77.0	108.0	108.6

a. The errors are obtained using one standard deviation from average of all the surface coverage considered in this work.

b. The uncertainties in desorption energy due to the uncertainties in contact angle measurements are less than 10 k_BT for all NPs considered.

2.3 Micro Wilhelmy Plate Algorithm

To calculate the interfacial tension while accounting for NP-NP interactions, we developed an algorithm that we define 'Micro Wilhelmy Plate' (MWP) method. The interfacial tension obtained from calculations using the MWP algorithm is identified as γ_M, for 'mechanical' interfacial tension, to distinguish it from predictions obtained using Eq. (1). The algorithm is a numerical implementation of the experimental Wilhelmy plate method.[33] In brief, as schematically shown in Fig. 2, a detection plate with perimeter l is equilibrated at the interface. Then a perturbation force F_p is applied, forcing the detection plate into the oil phase by a given offset. By measuring the magnitude of F_p and the contact angle imposed on the detection plate (θ), the interfacial tension is obtained using the Wilhelmy equation:

$$\gamma_M = \frac{F_p}{l \cdot \cos\theta} \qquad (7)$$

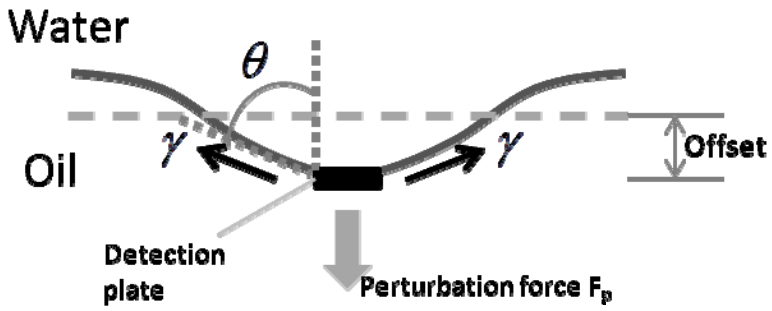

Figure 2. Schematic illustration of Micro Wilhelmy Plate algorithm (MWP). The detection plate (rectangle) is pulled into the oil phase from the original interface (dashed line) by applying a perturbation force F_p. By measuring the contact angle (θ) and the magnitude of the perturbation force, the interfacial tension (γ_M) can be calculated using Eq. (7)

The typical simulation setup for conducting calculations within the MWP algorithm is illustrated in Fig. 3. First a simulation box, containing water and decane, with dimensions $30\times30\times80R_c^3$ is equilibrated for 1,000,000 steps. Decane forms a layer of thickness 40 R_c along the Z direction between two layers of water (one layer if the periodic boundary is considered). The system contains roughly 100,000 water beads and 50,000 decane molecules. After equilibration, nanoparticles and detection plate are inserted at both interfaces. Then the system is equilibrated for another 2,000,000 steps to relax the interfacial structure of the NPs before carrying out the MWP measurement. The system volume is kept constant during MWP calculations. MWP simulations are carried out in the NVT ensemble.

The detection plate in our MWP algorithm is modeled as a single layer of dp beads of dimension $30\times3R_c^2$ lying flat on the center of both upper and lower interfaces. The interaction parameters for the detection plate a_{dp-j} are chosen arbitrarily as listed in Table 1. Sample simulations were performed by setting a_{dp-w} = a_{dp-o} =200 k_BT/R_c and a_{dp-ap} = a_{dp-p} =131.5 k_BT/R_c. It was found that, within these limits, the choice of interaction parameters for the detection plate does not have a significant influence on the surface tension measurement.

The detection plate is effectively infinite along the X direction. This guarantees that the algorithm creates an interface that only curves in one dimension. The width of the detection plate is large enough to prevent its detachment from the interface during the MWP calculations, and small enough not to affect significantly the amount of nanoparticles adsorbed at the interface. For the systems considered here, the optimal width of the detection plate was found to be 3 R_c. During MWP calculations, the detection plate is deflected 2 R_c into the oil phase. It is observed that for the system dimension used in this study, deflections above 3 R_c will create too large a perturbation over the entire interface, which will render the calculation inaccurate. A deflection of 2 R_c is chosen in order to minimize the perturbation to the interface while easing the contact angle (θ) measurement. Larger box sizes would be required for larger deflections.

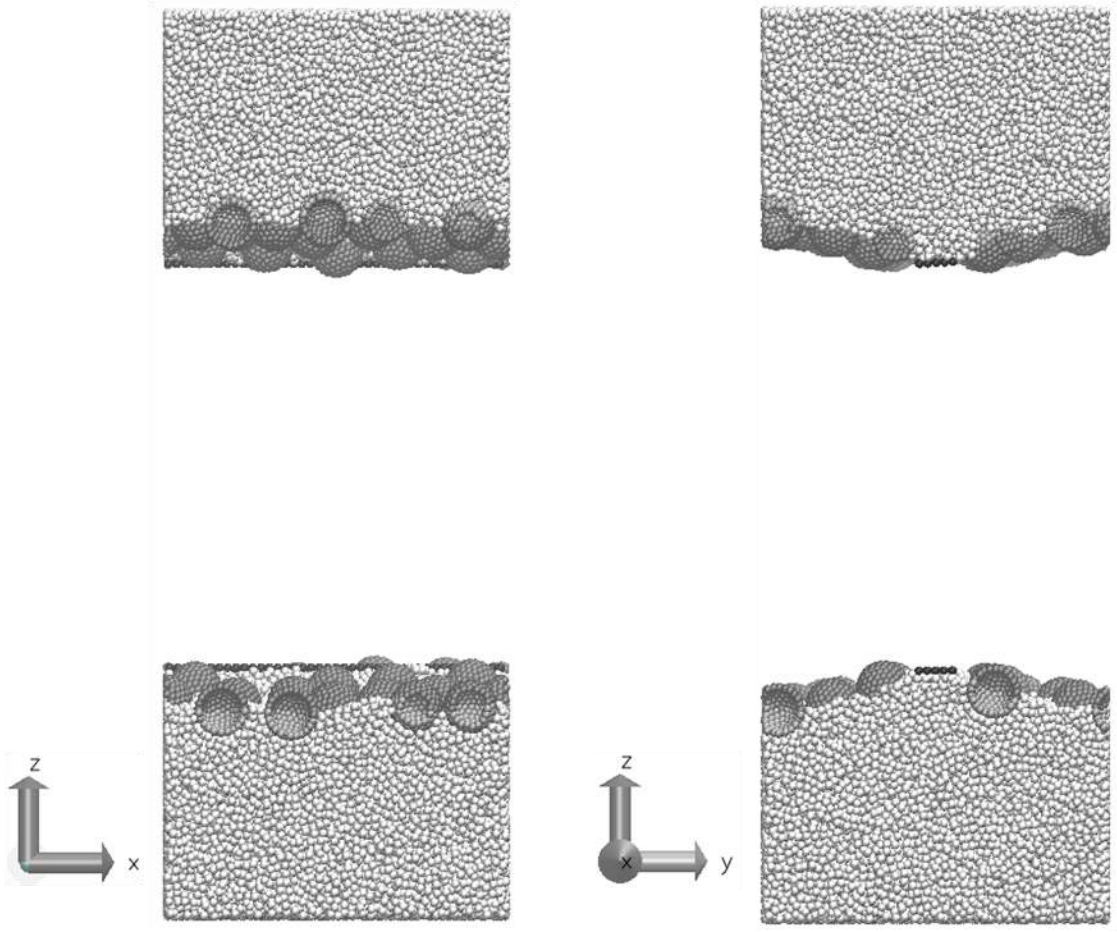

Figure 3. Illustration of the MWP algorithm. Left and right panels are for front and side views, respectively. White, light gray, dark gray, and black spheres represent water beads, polar beads (p), apolar beads (ap) and dp beads, respectively. The oil phase is not shown for clarity. There are twenty-five 0.50JP NPs adsorbed on each interface, yielding a surface coverage of 33.6 R_c^2.

To validate the MWP algorithm we computed the tension of a water-oil interface in the presence of model surfactants. The surfactants used are composed of one hydrophilic (head) bead (h) and one hydrophobic (tail) bead (t), connected by one harmonic spring. The interaction parameters for the head bead are set equal to those for the water beads. Those for the tail bead were set equal to those for the oil beads.

The results are compared to those obtained implementing the Kirkwood-Buff pressure tensor method (KB),[18] which has been widely used to calculate the interfacial tension for surfactant systems in both molecular dynamics and DPD simulations.[34, 35] Within the pressure tensor method aqueous and organic phases are at contact yielding unperturbed planar interfaces along the X and Y directions of the simulation box. In these simulations the Berendsen pressure coupling (NPT ensemble) was applied to the Z direction of the simulation box with reference pressure of 121.35 $k_B T/R_c^3$ and damping parameter of 1000 time steps. The system pressure components (P_{xx}, P_{yy} and P_{zz}) are recorded and used to calculate the interfacial tension as $\gamma = \frac{1}{2}\left\langle \left(P_{zz} - \frac{P_{xx}+P_{yy}}{2} \right) \right\rangle L_z$, where L_z is the length of the simulation box along the Z dimension. The same system dimensions were used as for the MWP calculations. The system pressure components, which are averaged over the entire simulation box, are obtained from the outputs of the simulation package.

In Fig. 4 we plot the surface tension reduction calculated using both our MWP method and the pressure tensor method as a function of surfactants surface coverage. The results show good agreement between the two methods implemented.

We tested the MWP algorithm for surfactant systems in which the surfactant molecular structure was kept unchanged, but the interaction parameters were changed. The interaction parameters for head-water (a_{h-w}) and tail-oil (a_{t-o}) interactions are increased by a certain amount (Δa), while those for head-oil (a_{h-o}) and tail-water (a_{t-w}) interactions were decreased by Δa. The resultant interaction parameters are reported in Table 3. In Fig. 5 the surface tension reduction as calculated by using either the MWP or the KB algorithms is plotted as a function of Δa. For these calculations the surface area was kept constant at 0.936 R_c^2 per surfactant molecule. The results obtained with the two methods are found in good agreement.

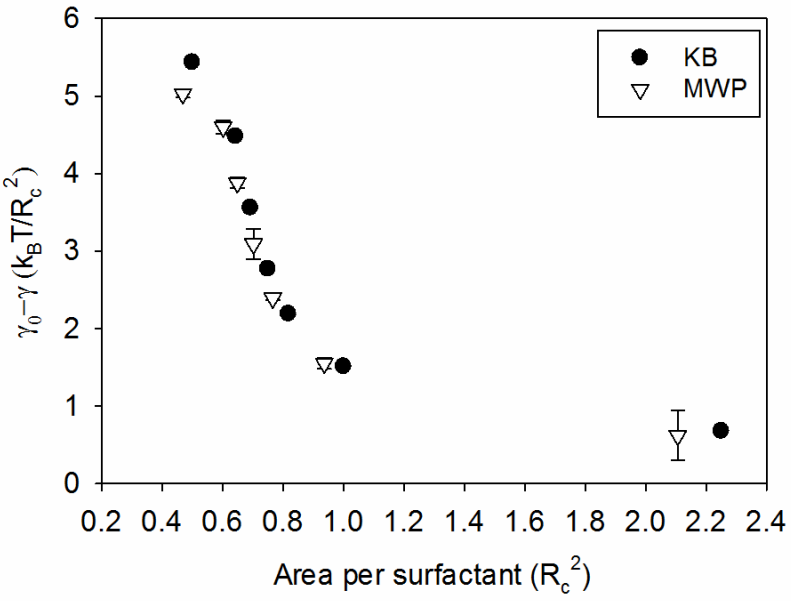

Figure 4. Surface tension reduction obtained using the MWP (empty triangles) and the pressure tensor algorithms (black circles) as a function of interfacial area per surfactant molecule. The uncertainties are obtained as one standard deviation from the average of three simulations. The error bars for the pressure tensor method are smaller than the symbols. The offset of the detection plate is set to 2 R_c for all the MWP measurements.

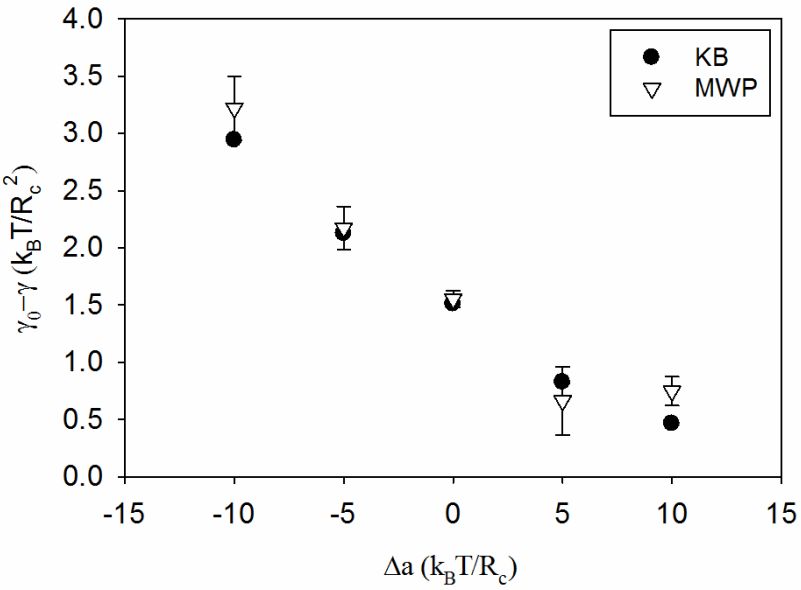

Figure 5. Surface tension reduction measured using the MWP (empty triangles) and KB algorithms (black circles) as a function of Δa . The error bars are obtained as one standard deviation from the average of three simulations. The error bars for the KB method are smaller than the symbols. The offset of the detection plate is set to 2 R_c for all the MWP measurements. The interaction parameters correspondent to each Δa are listed in Table 2.

Table 3. Modified a_{h-w}, a_{t-w}, a_{h-o} and a_{t-o} interaction parameters as a function of Δa. Interaction parameters and Δa are all expressed in $k_B T / R_c$.

Δa	**-10**	**-5**	**0**	**5**	**10**
a_{h-w}	121.5	126.5	131.5	136.5	141.5
a_{t-w}	208.5	203.5	198.5	193.5	188.5
a_{h-o}	208.5	203.5	198.5	193.5	188.5
a_{t-o}	121.5	126.5	131.5	136.5	141.5

We point out that the pressure-tensor method was not implemented to calculate the interfacial tension in the presence of nanoparticles because when the nanoparticles are present the direction Z of the simulation box does not always correspond to the direction perpendicular to the interface, altered by the solid nanoparticles. In all tested cases, the MWP algorithm yields results in excellent agreement with those obtained implementing the KB method.

2.4 NP-NP Interactions at the Water-Decane Interface

To estimate the force profile between two NPs at the interface, we built a smaller system of dimensions $15\times15\times11R_c^3$ with 2 NPs on one interface. Simulations were repeated for selected cases in simulation boxes of size $20\times20\times11R_c^3$, and no difference was observed, when statistical uncertainty was considered, between those results and the ones presented here. The NPs were connected by one harmonic spring with force constant of 15,000 $k_B T / R_c$. Representative simulations were conducted with the weaker force constant of 10,000 $k_B T / R_c$. No major effect of the spring constant was observed in the results obtained. The equilibrium length of the spring was set equal to the distance between two NPs at $t = 0$. The original distance between two NPs ($t = 0$) was varied systematically from 4.1 R_c to 7 R_c using intervals of length 0.1 R_c. At each separation, the system was first equilibrated for 10,000 steps and then 150,000 steps were performed for production. The effective NP-NP force was estimated at each separation by comparing the actual and equilibrium lengths of the spring, and by using the

spring constant to obtain the force from the spring length. The force so obtained was recorded every 150 steps during the 150,000 time steps of production. Thus 1,000 data points were generated at each separation, and averaged to yield the average NP-NP force. The procedure was repeated twice within the NP-NP separation range between 4.1 and 6.0 R_c. No significant difference was observed between the two sets of data. Because the simulated effective NP-NP force was low at large distances, we did not replicate measurements in the range of NP-NP distances 6 to 7 R_c. The raw simulation data were then interpolated using spline functions to obtain force-distance curves, as discussed below.

3 Results and Discussion

In Fig. 6 we plot the interfacial tension reduction ($\gamma_0 - \gamma_C$) as predicted by applying Eq. (1) for the water-decane interface in the presence of various NPs. The results are shown as a function of the surface area per NP. As the surface area per NP decreases, the NP density at the interface increases. For clarity, the interfacial tension reduction is shown only for selected values of the surface areas per NPs. The results in Fig. 6 suggest that Eq. (1) yields a gradual increase of the interfacial tension reduction as the NPs become more and more dense at the interface. Based on Fig. 6, the interfacial tension reduction strongly depends on NP type. Those NPs with large desorption energy show large interfacial tension reduction. For example, because 0.50JP and 0.75JP NPs have the largest desorption energy among all the NPs considered here, they yield the largest interfacial tension reduction. 1.00HP and 0.25JP have identical desorption energies, thus they should be identically capable to reduce the interfacial tension. It is expected that the latter NPs are capable of reducing the interfacial tension by 2 $k_B T / R_c^2$ even at the largest interfacial area per NP considered (56 R_c^2). Note that R_c is the DPD cutoff distance (see Simulation Methods and Algorithms), and that in the systems considered here the NPs radius is 2 R_c.

It should be pointed put that the desorption energy used for the calculations shown in Fig. 6 is considered to be constant, for a given NP, independently on the number of NPs at the interface. This simplification is consistent with Eq. (1), although it is expected that the desorption energy will depend on NP-NP interactions. These are expected to impact the interfacial tension significantly when the NP coverage increases, as shown below using the MWP algorithm. It

should also be pointed out that the results for the interfacial tension reduction shown in Figure 6 are within the range of experimentally observed data.

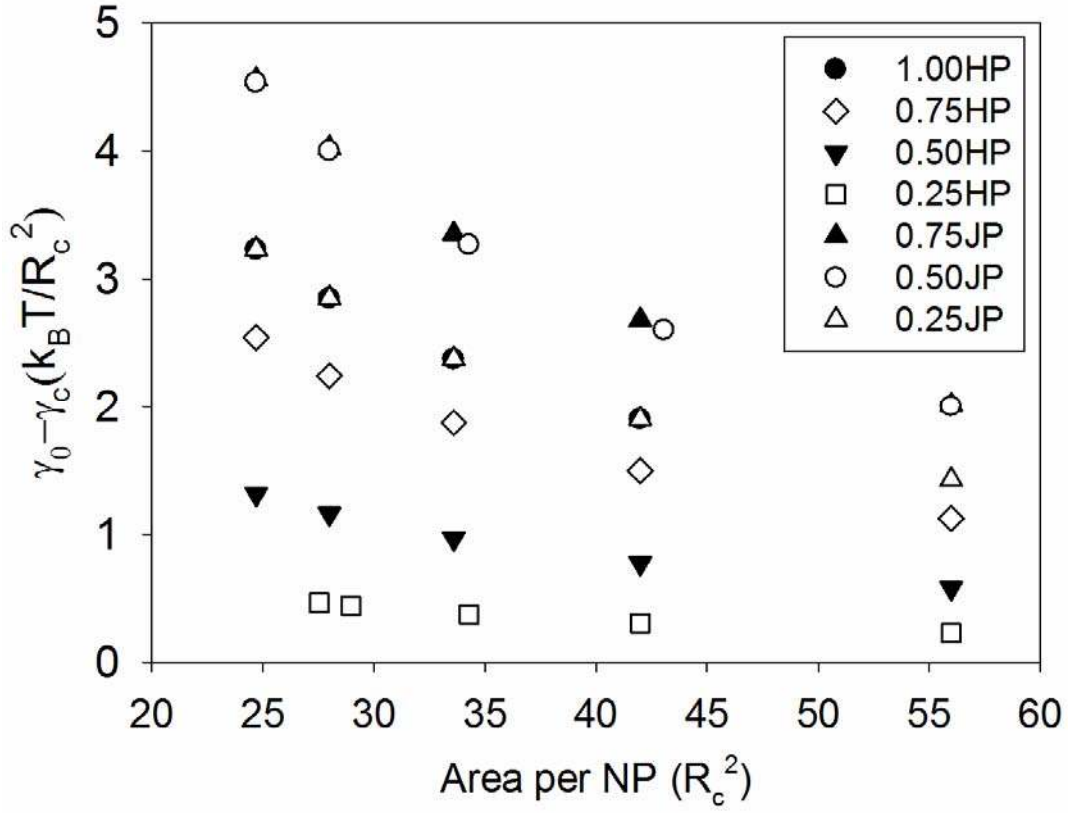

Figure 6. Interfacial tension reduction as calculated by Eq. (1) plotted as function of the interfacial area per NP. The error bars (not shown) are smaller than the symbols. Different symbols represent results obtained for different NPs.

As opposed to the results just discussed, in Fig. 7 we summarize the interfacial tension reduction ($\gamma_0 - \gamma_M$) in the presence of the various NPs as calculated from the MWP algorithm. Selected error bars are obtained as the one standard deviation from the average of 3 independent simulations (originated with different initial configurations, and different seeds for random initial velocities and force distributions). Due to limited computational resources, we only calculated the error bars for systems containing 0.50HPs and 0.50JPs.

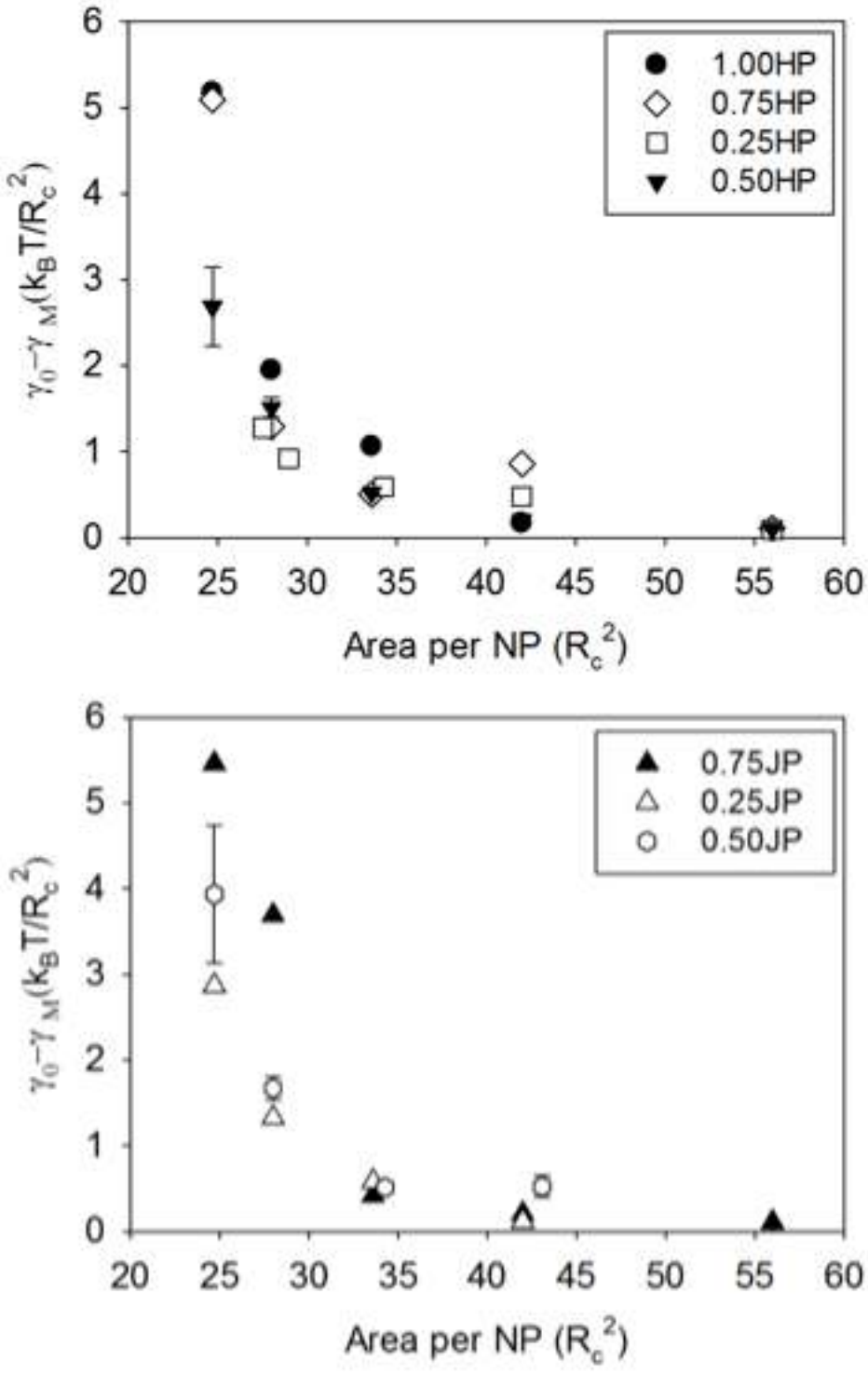

Figure 7. Interfacial tension reduction predicted using the MWP algorithm as a function of the interfacial area per NPs. Different symbols represent results for different NPs, as in Fig. 6. To ease visualization, results for homogeneous NPs are shown in the top panel, those for Janus NPs on the bottom panel. Only selected error bars are calculated because of computing power limitations. These are obtained as one standard deviation from the average.

The interfacial tension reduction estimated with the MWP approach is much lower than that estimated with Eq. (1) except at the largest surface coverage considered. This could be due, at least in part, to uncertainties in estimating the desorption energies, which are not used explicitly by the MWP method. At larger areas per NP (lower NP surface density) the interfacial tension reduction reduces only slightly as the interfacial area per NPs increases, regardless of the NP type. When the area per NP is above $40R_c^2$ little, if any, change in the interfacial tension is observed compared to values obtained at the bare water-decane interface. The qualitative trend predicted by the results in Fig. 7 appears to be consistent with experimental observations, according to which noticeable reductions in interfacial tensions, when observed, tend to occur at rather large nanoparticles loadings. When the interfacial area per NP is less than ~$30R_c^2$, the interfacial tension reduction predicted in Fig. 7 increases very fast as the interfacial area per NP decreases. At the smallest interfacial areas per NP considered, MWP predictions suggest that the reductions in interfacial tension in the presence of 0.75JPs, 0.75HPs, and 1.00HPs are similar. This is surprising when compared to data shown in Fig. 6, where the results obtained for these three NPs differ significantly, as the desorption energies estimated for 1.00HPs and 0.75HPs are much lower than that estimated for 0.75JP NPs (see Table 2). This observation suggests that, according to our MWP calculations, the NP desorption energy is not directly associated with the interfacial tension reduction.

To rationalize the differences between interfacial tension reductions estimated following the two approaches above, inspired by Clegg et al.,[36] we report in Fig. 8 a schematic of the total surface free energy as a function of the area of the interface for the various systems considered. The expected surface free energy as a function of interfacial area when no NPs are present is shown as dash-dot line. The slope of this line is the interfacial tension of the bare liquid-liquid interface, γ_0. The dashed line in Fig. 8 schematically represents changes in the total surface free energy in the presence of NPs as predicted by Eq. (1). The continuous lines represent changes in the total surface free energy as captured by the MWP algorithm. In this case, when NPs are present at the interface, if the area of the interface increases by amounts smaller than $a_0R_c^2$ the newly created interface is bare water-decane interface. [In the schematic of Fig. 8 it is assumed that the number of interfacial NPs remains constant until a sufficient amount of interfacial area ($a_0R_c^2$) is available that allows the insertion of one new NP at the interface while maintaining

the initial NP surface density.] When a sufficient amount of interfacial area has been created to allow one additional NP to adsorb, the amount of surface free energy decreases in an amount correspondent to the NP adsorption energy (vertical dotted lines in Fig. 8). If the MWP algorithm is applied under conditions at which no additional NP adsorbs at the interface while the calculation is being conducted, it should yield the slope of the black continuous lines. This slope will depend on a number of phenomena, including for example NP-NP interactions at the interface. When repulsive, such interactions (which facilitate the expansion of the interface) are known to be capable of reducing the interfacial tension in Langmuir-Blodgett type experiments.[37, 38] This and other effects would result in different functional forms for the continuous lines. For small increases in the interfacial area we expect that the slope of the solid lines (i.e., predictions based on the MWP algorithm) better represents the system interfacial tension than the slope of the dashed line [i.e., predictions based on Eq. (1)].

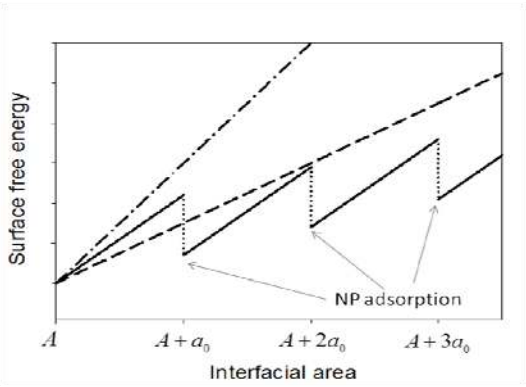

Figure 8. Schematic representing the variation in surface free energy as the interfacial area A increases. For a description of the various symbols and lines please refer to the text. a_0 is the interfacial area necessary for one NP to adsorb. γ_0, γ_c, and γ_M are obtained as the slopes of the dash-dotted, dashed, and solid lines, respectively.

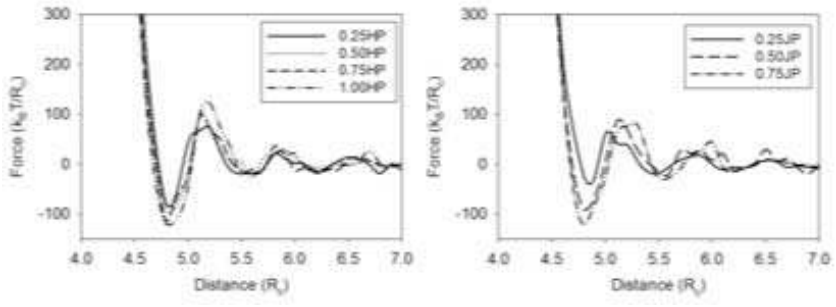

Figure 9. Average NP-NP forces at the interface plotted as function of the separation between the NPs center. The left and right panels are for homogeneous and Janus NPs, respectively.

The argument in Fig. 8 suggests that NP-NP interactions are responsible for the discrepancies observed when results in Fig. 6 are compared to those in Fig. 7. To support this argument we calculated NP-NP forces at the water-decane interface. In Fig. 9 we report simulated NP-NP force distance curves. The statistical uncertainty at each data point is within $5\,k_BT / R_c$. To reduce errors in the interpolation procedure a separation of 0.1 R_c was used between adjacent data points. Large repulsive interactions are experienced by two NPs when they are closer than 4.5 R_c and an attractive well is in general observed at ~ 4.8 R_c. As the cutoff in DPD interactions is set at 1.0 R_c in our simulations, many maxima and minima observed in the force-distance profiles of Fig. 9 are due to solvent effects, including depletion interactions[39, 40] and layering.

To relate, at least qualitatively, the interfacial tension reduction of Fig. 7 to NP-NP interactions at the interface we calculate the two-dimensional pressure among the NPs by applying the virial theorem: [41, 42]

$$\Pi A = Nk_BT + \left\langle \frac{1}{2}\sum_{i=1}^{N}\sum_{j>1}^{N} r_{ij}\cdot f_{ij} \right\rangle \qquad (8)$$

In Eq. (8), Π denotes the 2D pressure, A the interfacial area, f_{ij} and r_{ij} the force and distance between nanoparticles i and j. To apply Eq. (8) we require f_{ij}, which is interpolated from the force profile calculations between two NPs at the interface (Fig. 9). Results for the 2D pressures for the various systems as a function of the surface area per NP are reported in Fig. 10. We report both best-fit curves and raw simulation data. The effective NP-NP force is likely to depend on NP coverage. This was not accounted for in our calculations, as only pair-wise interactions were used for results shown in Fig. 10.

At a given NP density, the 2D pressure will depend on the distribution of the NPs on the interface, yielding the rather scattered results. The results for the 2D pressure obtained for each NP type at various coverages were fitted using the arbitrary function:

$$f(x) = \frac{c_1}{(x+c_2)^{c_3}} + c_4 \qquad (9)$$

In Eq. (9) c_1, c_2, c_3 and c_4 are fitting parameters. The fitting parameters obtained for each NP type, as well as the R^2 value indicating the statistical confidence in each fitting procedure are

reported in Table 4. As shown in Fig. 10, because the fitting curve misses many details shown by the simulated 2D pressure profiles, it is no surprise that the R^2 values shown in Table 4 reflect rather poor fitting. Given the high uncertainty in each 2D pressure, more sophisticated fitting functions than that expressed by Eq. (9) are not used. As a consequence, because of the large uncertainty, the conclusions from the 2D pressure calculations can only be taken as qualitative suggestions. The 2D pressure results show a dependence on the surface coverage that seems qualitatively similar to the one observed for the interfacial tension reduction shown in Fig. 7. Complete agreement between the two curves is not expected, because the MWP algorithm considered a slightly curved interface, which might affect NP-NP interactions, because of large uncertainties in calculating NP-NP force profiles at the interface, because of poor fitting of the 2D pressures to simulation data, and because the interfacial tension depends also on water-decane interactions, not included explicitly in the calculation of 2D pressures. However, the qualitative analogy between the results in Fig. 7 and those in Fig. 10 suggests that including NP-NP interactions is necessary for a correct estimation of interfacial tension reduction in Pickering emulsions. The relevance of 2D pressure is supported by experimental data intended to characterize the mechanical response of particle-laden interfaces.[43]

It should also be pointed out that in correspondence to large reductions in surface tensions our results showed the appearance of hexagonal arrangements of NPs at the interfaces. No details on such structures are provided for brevity, but such structures were observed when simulation boxes of size both $25\times25\times80R_c^3$ and $30\times30\times80R_c^3$ were employed.

Table 4. Fitting parameters and R^2 value of the fitting curves for the 2D pressure data.

	0.25HP	**0.50HP**	**0.75HP**	**1.00HP**	**0.25JP**	**0.50JP**	**0.75JP**
c_1	185855.8	185855.8	185855.8	185855.8	185855.8	185855.8	185855.8
c_2	-2.173	7.364	-10.497	-2.173	-7.664	33.205	-13.342
c_3	3.500	3.152	4.220	3.500	3.758	2.726	4.862
c_4	0.0667	-0.226	0.0333	0.0666	-0.0743	-0.785	0.434
R^2	0.48	0.73	0.90	0.78	0.75	0.75	0.89

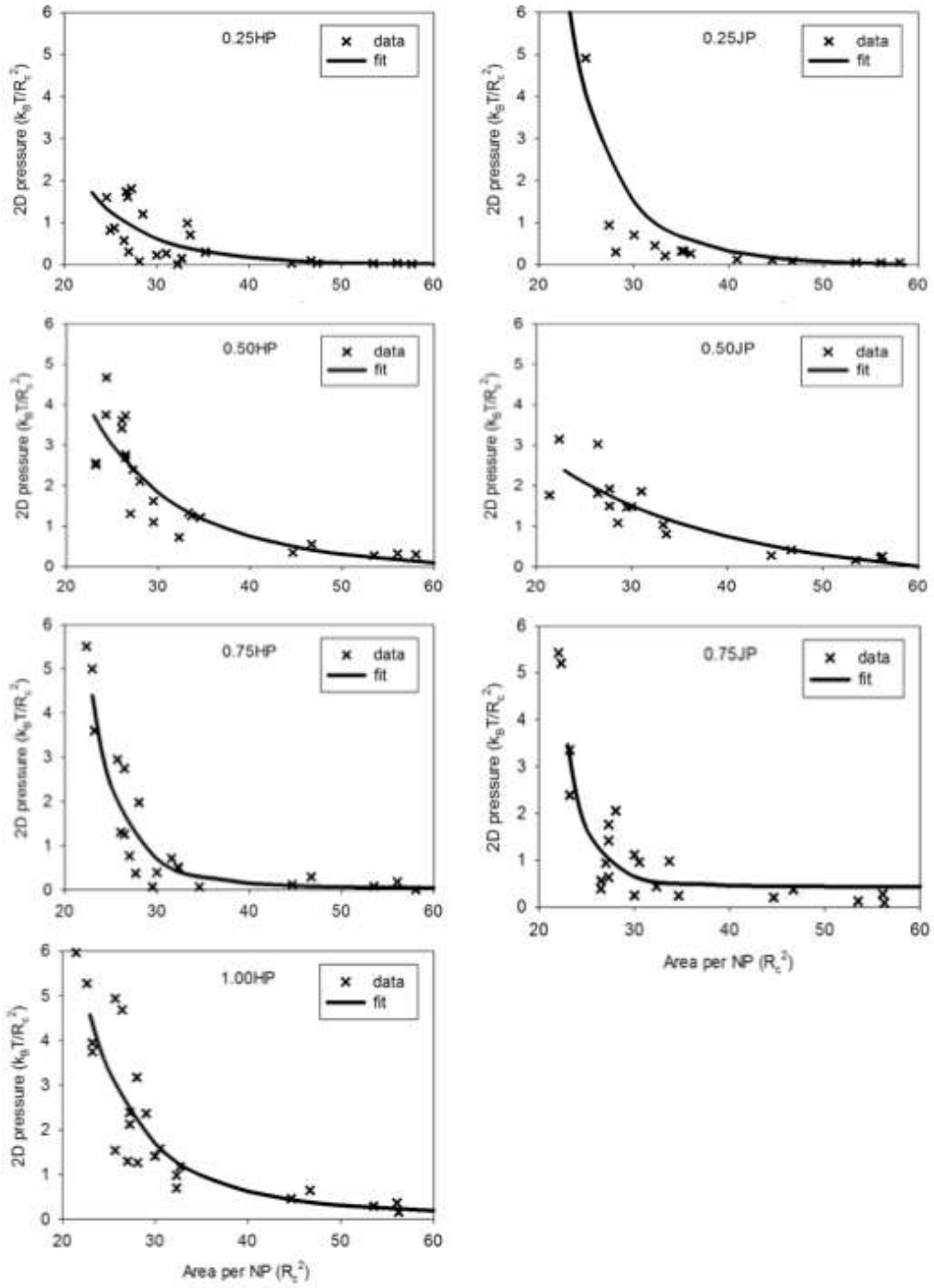

Figure 10. Two-dimensional pressures calculated using Eq. (8) plotted as a function of area per NP. The solid lines are fitting curves using the arbitrary function (Eq. (9)) through the 2D pressure data (crosses). Different panels are for different nanoparticles. Panels on the left are for homogeneous NPs, those on the right for Janus NPs. Statistical analysis is provided in Table 4. Lines are fitting curves.

The results presented so far suggest that to correctly predict interfacial tension reductions it is necessary to include NP-NP interactions, especially at high loadings of NPs at the interface. At this point it is desirable to revisit the experimental results summarized in the introduction and see if a unifying picture can be attained.

A number of experiments report no changes in the interfacial tension when particles are present.[3, 4] We suggest that these observations are due to low surface density of particles or/and weak particle-particle interactions at the interfaces of interest, which induce low surface pressure. Since strong repulsive interactions can lead to ordered configurations,[44] a crystalline structure of interfacial particles could be a plausible indication of high surface pressure. This could explain why Okubo et al.[3] observed interfacial tension reduction when crystalline structures were observed and not otherwise, and why Vignati et al.,[4] whose images suggest liquid-like NPs organization at interfaces, did not report interfacial tension reductions.

Our results suggest that the interfacial tension is not a direct function of the desorption energy of the NPs. However, because our results suggest that the interfacial tension depends strongly on the NPs coverage, and because the NPs coverage depends on the NPs affinity to the interface,[45] our results are consistent with a dependency of the interfacial tension on NPs desorption energy, although indirectly. Increasing the size of the NPs can significantly increase the desorption energy, leading to larger surface coverage, and therefore larger interfacial tension reductions.[19, 45] Similarly, the large interfacial tension reduction often reported for Janus NPs could also be attributed to the larger adsorption energy compared to those typical for homogeneous NPs.[10] As significant interfacial tension reductions are observed when strong particle-particle repulsions are present, if the adsorption energy is not sufficiently high, the nanoparticles will not yield surface densities sufficient to produce noticeable interfacial tension reductions. Preliminary simulations investigating the adsorption of NPs at interfaces (not shown here) indeed suggest that NPs with small desorption energy (e.g. homogeneous NPs) yield lower surface coverage than those required to induce large interfacial tension reductions. Janus NPs typically have high adsorption energies, and therefore are expected to pack densely at an interface, achieving large interfacial tension reductions.

Because NP-NP repulsions can increase in the presence of electrostatic effects, more significant reductions in interfacial tension are expected for charged systems,[3, 11] although such effects are expected to be very sensitive to salt concentration.[19, 46] Solution pH can alter both the surface

properties of the nanoparticles (e.g., their 'hydrophobicity'),[47] as well as NP-NP interactions[48]. Silica NPs adsorb more strongly at interfaces at low pH, which could lead to crowding and interfacial tension reductions, as reported by Blute et al.[5] For capped gold nanoparticles, high pH could promote NP-NP repulsion, yielding pronounced interfacial tension reductions.[46]

If repulsive NP-NP interactions lead to reductions in interfacial tension, attractive interactions could be responsible for increases in interfacial tension. This interpretation is in agreement with Johnson and Dong,[1] who proposed that the increase in interfacial tension they observed for charge-stabilized TiO_2 dispersions at high pH and high nanoparticle concentrations might be due to attractive capillary interactions between NPs at the interface.

When particles decorated with various molecules are considered, the effect on the interfacial tension will be related to the effective particle-particle interactions. As such interactions are expected to become repulsive for brushes, the interfacial tension is expected to decrease.[11, 49, 50]

4 Conclusions

In summary, we have conducted a number of dissipative particle dynamics simulations to calculate the interfacial tension reduction at the water-decane interface due to the presence of a number of different nanoparticles. The nanoparticles considered include homogeneous and Janus ones. We have compared values for the interfacial tension reduction estimated implementing a newly developed algorithm, which we identify as the 'Micro Wilhelmy Plate' algorithm, MWP, to those we can estimate assuming that nanoparticles do not interact with each other at the interface. We have found that the results obtained from the two approaches differ substantially from each other, and we argue that accounting for nanoparticle-nanoparticle interactions is essential for achieving a correct phenomenological picture of the behavior of nanoparticles at liquid-liquid interfaces, especially when high loadings of nanoparticles are considered. While a number of effects are certainly not included in our model, the molecular insights provided by our calculations provide a tentative unifying interpretation of a number of experimental observations reported in the literature.

5 Acknowledgements

This work was supported, in part, by the NSF award # CBET-1033129. Generous allocations of computing time were provided by the OU Supercomputing Center for Education and Research (OSCER) and by the National Energy Research Scientific Computing Center (NERSC) at Lawrence Berkley National Laboratory.

6 References

1 L. C. Dong and D. Johnson, Langmuir **19**, 10205 (2003).
2 B. P. Binks, Current Opinion in Colloid & Interface Science **7**, 21 (2002).
3 T. Okubo, Journal of Colloid and Interface Science **171**, 55 (1995).
4 E. Vignati, R. Piazza, and T. P. Lockhart, Langmuir **19**, 6650 (2003).
5 I. Blute, R. J. Pugh, J. van de Pas, et al., Colloids and Surfaces a-Physicochemical and Engineering Aspects **337**, 127 (2009).
6 V. Saeid, P. Arup, J. Abhishek, et al., Nanotechnology **20**, 185702 (2009).
7 S. Vafaei, T. Borca-Tasciuc, M. Z. Podowski, et al., Nanotechnology **17**, 2523 (2006).
8 I. Akartuna, A. R. Studart, E. Tervoort, et al., Langmuir **24**, 7161 (2008).
9 U. T. Gonzenbach, A. R. Studart, E. Tervoort, et al., Langmuir **22**, 10983 (2006).
10 N. Glaser, D. J. Adams, A. Boker, et al., Langmuir **22**, 5227 (2006).
11 N. Saleh, T. Sarbu, K. Sirk, et al., Langmuir **21**, 9873 (2005).
12 Z. Yang, X.-P. Long, and Q.-X. Zeng, Polymer **52**, 6110 (2011).
13 L. S. De Lara, M. F. Michelon, and C. O. Metin, Journal of Chemical Physics **136**, 164702 (2012).
14 R. J. K. U. Ranatunga, C. T. Nguyen, and B. A. Wilson, Soft Matter **7**, 6942 (2011).
15 M. Luo and L. L. Dai, Journal of Physics: Condensed Matter **19**, 375109 (2007).
16 F. W. Sears and M. W. Zemansky, *University physics* (Addison-Wesley, Reading, Mass.,, 1970).
17 P. Somasundaran, Science & Technology Libraries **22**, 189 (2001).
18 J. G. Kirkwood and F. P. Buff, Journal of Chemical Physics **17**, 338 (1949).
19 K. Du, E. Glogowski, T. Emrick, et al., Langmuir **26**, 12518 (2010).
20 E. Moeendarbary, T. Y. Ng, and M. Zangeneh, International Journal of Applied Mechanics **1**, 737 (2009).
21 R. D. Groot and K. L. Rabone, Biophysical Journal **81**, 725 (2001).
22 R. D. Groot and P. B. Warren, Journal of Chemical Physics **107**, 4423 (1997).
23 A. Maiti and S. McGrother, Journal of Chemical Physics **120**, 1594 (2004).
24 J. R. Partington, R. F. Hudson, and K. W. Bagnall, Nature **169**, 583 (1952).
25 M. Calvaresi, M. Dallavalle, and F. Zerbetto, Small **5**, 2191 (2009).
26 R. H. Hardin, N. J. A. Sloane, and W. D. Smith, Tables of spherical codes with icosahedral symmetry, published electronically at http://www.research.att.com/~njas/icosahedral.codes/.
27 J. Brandrup, E. H. Immergut, and E. A. Grulke, *Polymer handbook* (Wiley, New York, 1999).
28 A. Goebel and K. Lunkenheimer, Langmuir **13**, 369 (1997).
29 H. Fan, D. E. Resasco, and A. Striolo, Langmuir **27**, 5264 (2011).
30 S. Plimpton, Journal of Computational Physics **117**, 1 (1995).
31 B. P. Binks and P. D. I. Fletcher, Langmuir **17**, 4708 (2001).
32 S. Jiang and S. Granick, Journal of Chemical Physics **127** (2007).
33 Holmberg, *Handbook of Applied Surface and Colloid Chemistry* (John Wiley & Sons, 2002).
34 L. Shi, N. R. Tummala, and A. Striolo, Langmuir **26**, 5462 (2010).
35 V. V. Ginzburg, K. Chang, P. K. Jog, et al., Journal of Physical Chemistry B **115**, 4654 (2011).

[36] P. S. Clegg, E. M. Herzig, A. B. Schofield, et al., Langmuir **23**, 5984 (2007).
[37] S. Reculusa, R. Perrier-Cornet, B. Agricole, et al., Physical Chemistry Chemical Physics **9**, 6385 (2007).
[38] A. Deak, B. Bancsi, A. L. Toth, et al., Colloids and Surfaces a-Physicochemical and Engineering Aspects **278**, 10 (2006).
[39] S. Asakura and F. Oosawa, Journal of Polymer Science **33**, 183 (1958).
[40] F. Oosawa and S. Asakura, Journal of Chemical Physics **22**, 1 (1954).
[41] Z. Horvolgyi, A. Agod, and N. Nagy, Langmuir **23**, 5445 (2007).
[42] J. Z. Sun and T. Stirner, Langmuir **17**, 3103 (2001).
[43] C. Monteux, J. Kirkwood, H. Xu, et al., Physical Chemistry Chemical Physics **9**, 6344 (2007).
[44] B. P. Binks, Physical Chemistry Chemical Physics **9**, 6298 (2007).
[45] S. Kutuzov, J. He, R. Tangirala, et al., Physical Chemistry Chemical Physics **9**, 6351 (2007).
[46] S. Ferdous, M. Ioannidis, and D. Henneke, Journal of Nanoparticle Research **14**, 1 (2012).
[47] G. Gillies, K. Buscher, M. Preuss, et al., Journal of Physics-Condensed Matter **17**, S445 (2005).
[48] V. M. Gun'ko, V. I. Zarko, R. Leboda, et al., Colloids and Surfaces a-Physicochemical and Engineering Aspects **132**, 241 (1998).
[49] J. U. Kim and M. W. Matsen, Macromolecules **41**, 4435 (2008).
[50] W. B. Russel, D. A. Saville, and W. R. Schowalter, *Colloidal dispersions* (Cambridge University Press, Cambridge ; New York, 1989).